Pulsed laser deposition of high-quality μm-thick YIG films on YAG

A. Sposito,[1,*] T. C. May-Smith,[1] G. B. G. Stenning,[2] P. A. J. de Groot,[2] and R. W. Eason[1]

[1]*Optoelectronics Research Centre, University of Southampton, SO17 1BJ, Southampton, United Kingdom*
[2]*Physics and Astronomy, University of Southampton, SO17 1BJ, Southampton, United Kingdom*
**as11g10@orc.soton.ac.uk*

Abstract: We report the epitaxial growth of high-quality μm-thick yttrium iron garnet (YIG) films on yttrium aluminium garnet (YAG) substrates by pulsed laser deposition (PLD). The effects of substrate temperature and oxygen pressure on composition, crystallinity, optical transmission and ferromagnetic resonance (FMR) linewidth have been investigated. An FMR linewidth as low as 1.75 mT at 6 GHz was achieved by depositing YIG on YAG substrates with (100) orientation at a substrate temperature of ~1600 K and with oxygen pressure of ~1 Pa.

OCIS codes: (160.3820) Magneto-optical materials; (310.1860) Deposition and fabrication.

References and links

1. R. W. Eason, *Pulsed Laser Deposition of Thin Films – Applications-led Growth of Functional Materials* (Wiley Interscience, 2007).
2. N. A. Vainos, C. Grivas, C. Fotakis, R. W. Eason, A. A. Anderson, D. S. Gill, D. P. Shepherd, M. Jelinek, J. Lancok, and J. Sonsky, "Planar laser waveguides of Ti:sapphire, Nd:GGG and Nd:YAG grown by pulsed laser deposition," Appl. Surf. Sci. **127-129**, 514–519 (1998).
3. H. Dötsch, N. Bahlmann, O. Zhuromskyy, M. Hammer, L. Wilkens, R. Gerhardt, P. Hertel, and A. F. Popkov, "Applications of magneto-optical waveguides in integrated optics: review," J. Opt. Soc. Am. B **22**(1), 240–253 (2005).
4. G. B. G. Stenning, G. J. Bowden, L. C. Maple, S. A. Gregory, A. Sposito, R. W. Eason, N. I. Zheludev, and P. A. J. de Groot, "Magnetic control of a meta-molecule," Opt. Express **21**(2), 1456–1464 (2013).
5. S. A. Manuilov, R. Fors, S. I. Khartsev, and A. M. Grishin, "Submicron $Y_3Fe_5O_{12}$ film magnetostatic wave band pass filters," J. Appl. Phys. **105**(3), 033917 (2009).
6. H. Nishihara, M. Haruna, and T. Suhara, *Optical Integrated Circuits* (McGraw-Hill Professional, 1989).
7. L. Bi, J. Hu, P. Jiang, D. H. Kim, G. F. Dionne, L. C. Kimerling, and C. A. Ross, "On-chip optical isolation in monolithically integrated non-reciprocal optical resonators," Nat. Photonics **5**(12), 758–762 (2011).
8. S. Kahl and A. M. Grishin, "Pulsed laser deposition of $Y_3Fe_5O_{12}$ and $Bi_3Fe_5O_{12}$ films on garnet substrates," J. Appl. Phys. **93**(10), 6945–6947 (2003).
9. P. C. Dorsey, S. E. Bushnell, R. G. Seed, and C. Vittoria, "Epitaxial yttrium-iron-garnet films grown by pulsed-laser deposition," J. Appl. Phys. **74**(2), 1242–1246 (1993).
10. N. Kumar, S. Prasad, D. S. Misra, N. Venkataramani, M. Bohra, and R. Krishnan, "The influence of substrate temperature and annealing on the properties of pulsed laser-deposited YIG films on fused quartz substrate," J. Magn. Magn. Mater. **320**(18), 2233–2236 (2008).
11. A. Morimoto, Y. Maeda, T. Minamikawa, Y. Yonezawa, and T. Shimizu, "LPE-like growth of YIG ferrimagnetic thin films by pulsed laser ablation with molten droplets," Appl. Phys., A Mater. Sci. Process. **69**(7), S703–S706 (1999).
12. A. A. Jalali-Roudsar, V. P. Denysenkov, S. I. Khartsev, A. M. Grishin, N. Adachi, and T. Okuda, "Microwave and magneto-optic properties of pulsed laser deposited bismuth iron garnet films," IEEE Trans. Magn. **37**(4), 2454–2456 (2001).
13. S. Leitenmeier, T. Korner, J. Griesbauer, M. Herbort, A. Heinrich, and B. Stritzker, "Studies on the growth of epitaxial bismuth-substituted iron garnet on gadolinium gallium garnet single crystals by pulsed laser deposition," J. Cryst. Growth **310**(24), 5392–5401 (2008).
14. E. Popova, N. Keller, F. Gendron, M. Guyot, M. C. Brianso, Y. Dumond, and M. Tessier, "Structure and magnetic properties of yttrium-iron-garnet thin films prepared by laser deposition," J. Appl. Phys. **90**(3), 1422–1428 (2001).
15. C. J. Yang, S. W. Kim, and Y. S. Kim, "Polycrystalline $Y_3Fe_5O_{12}$ garnet films grown by a pulsed laser ablation technique," IEEE Trans. Magn. **30**(6), 4527–4529 (1994).
16. T. Boudiar, B. Payet-Gervy, M. F. Blanc-Mignon, J. Rousseau, M. Le Berre, and H. Joisten, "Magneto-optical properties of yttrium iron garnet (YIG) thin films elaborated by radio frequency sputtering," J. Magn. Magn. Mater. **284**, 77–85 (2004).

#185247 - $15.00 USD Received 12 Feb 2013; revised 14 Mar 2013; accepted 17 Mar 2013; published 16 Apr 2013

17. S. Y. Sung, X. Qi, and B. J. H. Stadler, "Integrating yttrium iron garnet onto nongarnet substrates with faster deposition rates and high reliability," Appl. Phys. Lett. **87**(12), 121111 (2005).
18. J.-M. L. Beaujour, A. D. Kent, D. W. Abraham, and J. Z. Sun, "Ferromagnetic resonance study of polycrystalline $Fe_{1-x}V_x$ alloy thin films," J. Appl. Phys. **103**(7), 07B519 (2008).
19. Y. Krockenberger, K.-S. Yun, T. Hatano, S. Arisawa, M. Kawasaki, and Y. Tokura, "Layer-by-layer growth and magnetic properties of $Y_3Fe_5O_{12}$ thin films on $Gd_3Ga_5O_{12}$," J. Appl. Phys. **106**(12), 123911 (2009).
20. K. A. Sloyan, T. C. May-Smith, M. Zervas, R. W. Eason, S. Huband, D. Walker, and P. A. Thomas, "Growth of crystalline garnet mixed films, superlattices and multilayers for optical applications via shuttered combinatorial pulsed laser deposition," Opt. Express **18**(24), 24679–24687 (2010).
21. B. M. Simion, G. Thomas, R. Ramesh, V. G. Keramidas, and R. L. Pfeffer, "Growth and characterization of ($Y_3Fe_5O_{12}$-$Bi_3Fe_5O_{12}$) heterostructures by pulsed-laser deposition," Appl. Phys. Lett. **66**(7), 830–832 (1995).
22. R. Swanepoel, "Determination of the thickness and optical-constants of amorphous-silicon," J. Phys. E **16**(12), 1214–1222 (1983).
23. L. Dobrzycki, E. Bulska, D. A. Pawlak, Z. Frukacz, and K. Woźniak, "Structure of YAG crystals doped/substituted with erbium and ytterbium," Inorg. Chem. **43**(24), 7656–7664 (2004).
24. D. Rodic, M. Mitric, R. Tellgren, H. Rundlof, and A. Kremenovic, "True magnetic structure of the ferrimagnetic garnet $Y_3Fe_5O_{12}$ and magnetic moments of iron ions," J. Magn. Magn. Mater. **191**(1-2), 137–145 (1999).
25. R. W. Damon and J. R. Eshbach, "Magnetostatic modes of a ferromagnet slab," J. Phys. Chem. Solids **19**(3–4), 308–320 (1960).
26. J. F. Dillon, "Magnetostatic modes in disks and rods," J. Appl. Phys. **31**(9), 1605–1614 (1960).

1. Introduction

Pulsed Laser Deposition (PLD) is a relatively inexpensive, simple, powerful and versatile deposition technique, which can be used to deposit a wide range of materials [1]. Cubic materials such as garnets have been successfully grown [2], some of which (e.g. yttrium iron garnet or YIG – $Y_3Fe_5O_{12}$) show magnetic and magneto-optic properties, which can be exploited for specific applications, such as Faraday rotators/isolators, magneto-optic memories and RF/microwave devices [3–5].

Properties such as coercivity and magnetic anisotropy can be varied to suit the final application: for instance waveguide magneto-optic rotators/isolators require the 'easy axis' to be in-plane [6], although other solutions are possible [7]; microwave devices need low coercivity, whereas magnetic recording media need high coercivity [5,8].

Magnetic properties of magneto-optic garnets can be easily tailored via PLD by changing the deposition conditions: for example, it has been demonstrated that coercivity and ferromagnetic resonance (FMR) linewidth of YIG films decrease with increasing substrate temperature [9,10]. However, there are several parameters involved in this film growth method, each of which can be varied over a wide range of values (e.g. laser frequency and energy, spot size and fluence, substrate temperature, gas pressure and distance between substrate and target). While some of these remain essentially fixed, e.g. the laser parameters (the excimer laser in our case), others are changed sequentially, e.g. substrate temperature and gas pressure, to establish optimum growth conditions.

Previous work was focused mainly on PLD of YIG on lattice-matched gadolinium gallium garnet (GGG – $Gd_3Ga_5O_{12}$) substrates [5,8,9,11]. However, previous reports [5,8,12,13] seem to suggest that film stress induces narrower FMR linewidth, in the YIG films. For this reason we have focused our attention on PLD of YIG on YAG substrates, which present a higher lattice mismatch than YIG on GGG, as will be shown later, lower cost and more ready availability than GGG substrates.

YIG films have also been deposited on various non-garnet substrates both by PLD [10,14,15] and sputtering [16,17]. However, YIG layers grown on non-garnet substrates are generally amorphous or poly-crystalline [10,14–17], thus requiring a further annealing step in order to improve crystallinity and optical and magnetic properties [10,16,17]. Also, very large lattice and/or thermal expansion coefficient mismatch between YIG films and non-garnet substrate can cause formation of cracks in μm-thick films during high-temperature depositions or thermal annealing [16].

We report on the optimization of deposition conditions of YIG films grown on YAG by PLD using measured values of the FMR linewidth, which were taken as a quality indicator. In particular the effects of lattice mismatch, substrate temperature and oxygen pressure on

#185247 - $15.00 USD Received 12 Feb 2013; revised 14 Mar 2013; accepted 17 Mar 2013; published 16 Apr 2013

composition, crystallinity, optical transmission and FMR linewidth have been investigated and will be the focus of the subsequent sections.

To our knowledge, we are the first to report high-quality μm-thick YIG films epitaxially grown by PLD on YAG, despite the considerable degree of lattice mismatch (3.1%) and μm-scale film thickness.

2. Experimental techniques

YIG films were deposited on 10 × 10 mm^2 1 mm-thick YAG and 0.5 mm-thick GGG substrates. A Coherent CompexPro 102F KrF excimer laser operating at 248 nm (20 ns pulse duration) was used to ablate a single-crystal YIG target and a Synrad J48-2W carbon dioxide (CO_2) laser operating at 10.6 μm (max. output power: 40 W) was used to heat the substrate during the deposition. The distance between target and substrate was fixed at 6 cm. Excimer laser fluence was set at around 3 J/cm^2 and laser repetition rate at 20 Hz. The other growth conditions, substrate temperature (T) and oxygen pressure (P_{O2}) were changed to allow a parametric evaluation of optimum growth.

The first films (samples Y1, Y6 and Y8-Y10) were grown under identical conditions (T ≈1300 K and P_{O2} ≈3.3 Pa) but on different substrates.

All subsequent depositions were performed on YAG (100)-oriented substrates under different conditions. Samples Y11-Y18 were grown at the same oxygen pressure (3.3 Pa) and different substrate temperatures; samples Y19-21 were grown at the same substrate temperature (~1600 K, the optimum value found from previous experiments), but different oxygen pressures.

YIG films were characterized by means of optical microscopy and SEM (Zeiss Evo 50) for surface analysis. Thickness measurements were performed by stylus profiler (KLA Tencor P-16). Compositional analysis was carried out by EDX (Oxford Instruments INCA PentaFETx3): the instrument was energy-calibrated with a cobalt stub before measurements and compositional analysis of stoichiometric YIG target and blank GGG and YAG substrates was performed and used for reference; the accuracy (absolute error) of our concentration measurements is estimated to be ±0.5%; oxygen concentration was assumed constant. Crystallographic analysis was performed by XRD (Bruker D2 Phaser, Siemens D5000 and D8). Transmission spectra were obtained by spectrophotometry (Varian Cary 500 Scan).

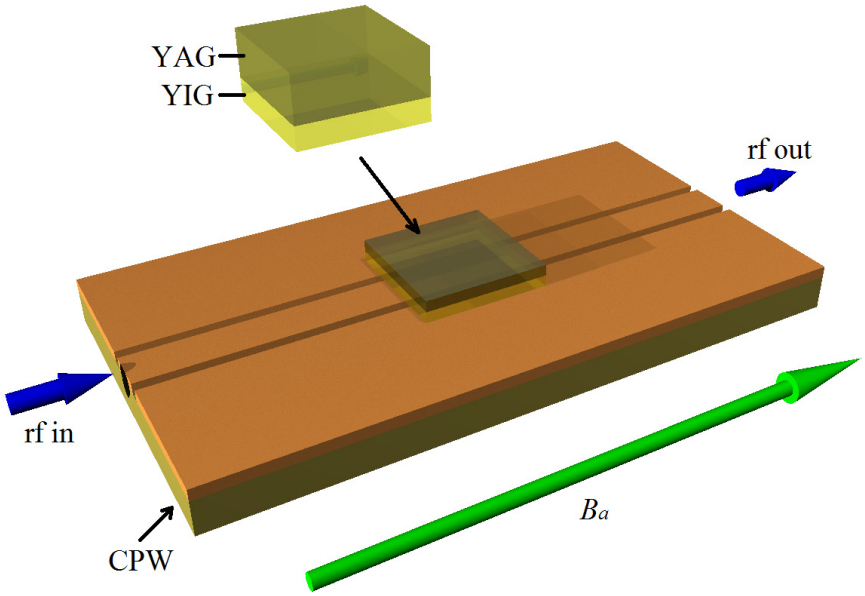

Fig. 1. Schematic of the FMR set-up. B_a is the applied magnetic field.

#185247 - $15.00 USD Received 12 Feb 2013; revised 14 Mar 2013; accepted 17 Mar 2013; published 16 Apr 2013

For FMR spectroscopy a DC magnetic field was applied via an electromagnet controlled by a bipolar power supply. The DC field strength was recorded using a Lakeshore 425 Gaussmeter. The RF field was achieved by excitation of microwaves from a 20 GHz E5071C Vector Network Analyzer (VNA) through low loss broadband cables passing through the centre of the electromagnetic pole pieces. These were connected to end-launch connectors which allowed for the transition from coaxial cable to a printed circuit board (PCB). The transition from coaxial to PCB allowed for the connection to the coplanar waveguide (CPW), which provided the RF field to the magnetic sample. The RF field and DC field were therefore mutually perpendicular, as required for FMR. The magnetic film was then placed with the film side towards the CPW, which ensured that there was good coupling from the microwave excitation to the magnetic film [18] (see Fig. 1). All values of FMR linewidth reported here were measured as the FWHM of the FMR absorption at a RF frequency of 6 GHz.

3. Results and discussion

3.1 YIG on different substrates

Firstly, YIG films were deposited on different substrates to see how they affect the film quality and magnetic properties. Table 1 shows the results of the characterization of samples Y1, Y6 and Y8-Y10: it can be seen that the highlighted sample Y6, deposited on YAG (100), has a lower FMR linewidth (ΔH) than any of the three films deposited on lattice-matched GGG substrates, which agrees with the previous findings reported in literature [5,8,12,13]. In fact, lattice mismatch between YIG and YAG is: $\Delta a/a_{SUB}$ = 3.1%, whereas $\Delta a/a_{SUB}$ = –0.056% for YIG on GGG, where: $\Delta a = (a_{FILM} - a_{SUB})$, a_{FILM} = lattice constant of the film, a_{SUB} = lattice constant of the substrate. Film orientation plays a role too in the magnetic properties, as shown already in [5,8,19].

Table 1. Substrates, FMR Linewidth (ΔH), Thickness (t) and Composition of Samples Y1, Y6 and Y8-Y10[a]

SAMPLE	Substrate	ΔH [mT]	t [μm]	Y at. %	Fe at. %	Y/Fe
Y1	GGG (111)	3.81	3	16.0	21.5	0.74
Y6	YAG (100)	3.37	1.2	17.0	20.0	0.85
Y8	YAG (100)	4.21	2.4	16.5	21.0	0.78
Y9	GGG (111)	4.42	2.75	16.5	20.5	0.80
Y10	GGG (100)	9.27	2.75	17.0	21.0	0.81

[a]The best sample in terms of FMR is highlighted in grey.

Crystallinity and epitaxial growth of all samples was confirmed by XRD. EDX analysis showed that all films are yttrium (Y) rich and iron (Fe) deficient, as reported in [5] for films grown on GGG (111) under similar deposition conditions – stoichiometric $Y_3Fe_5O_{12}$ should have: 15 at.% of Y and 25 at.% of Fe, i.e. a Y/Fe concentration ratio of 0.6.

We explain the better magnetic properties of our lattice-mismatched YIG/YAG samples, compared to our lattice matched YIG/GGG samples, with the same theory proposed in [12] for BIG films deposited on GSGG and NGSGG, that has also been confirmed in [5] for lattice-matched Fe-deficient and lattice-mismatched stoichiometric YIG films grown on GGG.

According to [12], a large lattice mismatch induces a strain that can be more easily relieved through misfit dislocations than the strain induced by a smaller lattice mismatch; consequently the films having a small lattice mismatch, such as BIG/NGSGG(111) ($\Delta a/a_{SUB}$ ≈0.13%), have larger strain and worse magnetic properties than films with higher lattice mismatch, such as BIG/GSGG(001) ($\Delta a/a_{SUB}$ ≈0.45%), as shown in Table 2, where data from [12] is compared.

#185247 - $15.00 USD Received 12 Feb 2013; revised 14 Mar 2013; accepted 17 Mar 2013; published 16 Apr 2013

Table 2. Comparison of Data from [12]

Samples	Lattice mismatch $\Delta a/a_{SUB}$	FMR linewidth ΔH [mT]	Coercivity H_C [kA/m]	Saturation magnetisation $4\pi M_S$ [kA/m]	Faraday rotation @ λ = 633 nm θ_F [deg/μm]
BIG/NGSGG(111)	0.13%	35	27.85	95.5	–6.7
BIG/GSGG(001)	0.45%	2.5	3.18	111.4	–7.8

From this same reasoning we infer that our YIG/YAG samples accommodate the strain induced by the large lattice-mismatch ($\Delta a/a_{SUB}$ ≈3.1%) better than our YIG/GGG samples ($\Delta a/a_{SUB}$ ≈–0.056%), thus inducing better magnetic properties.

Also, the better relief of the strain induced in YIG/YAG than in YIG/GGG can be explained by taking into account the thermal expansion coefficients (TEC, ρ) of the materials: $\rho_{YIG} = 10.4 \cdot 10^{-6}$ K^{-1}, $\rho_{YAG} = 7.2 \cdot 10^{-6}$ K^{-1}, $\rho_{GGG} = 8.96 \cdot 10^{-6}$ K^{-1}. The lattice-mismatch in YIG/YAG ($\Delta a/a_{SUB}$ ≈3.1%) causes a compressive strain; however, the TEC-mismatch in YIG/YAG ($\Delta\rho/\rho_{SUB}$ ≈44.4%) will cause a tensile stress that can compensate the lattice-mismatch-induced compressive strain during the cooling-down of the sample at the end of the deposition. As for YIG/GGG, the lattice-mismatch ($\Delta a/a_{SUB}$ ≈–0.056%) induces a tensile strain that will be increased even more by the TEC-mismatch ($\Delta\rho/\rho_{SUB}$ ≈16.1%) during the cooling-down of the sample after the film growth.

3.2 Optimization of substrate temperature

Subsequent samples Y11-Y18 were deposited on YAG (100) substrates at the same oxygen pressure (P_{O2} ≈3.3 Pa) and different substrate temperatures, as shown in Table 3 (best sample in grey). It can be seen that all samples are Fe-deficient, with an average Y/Fe ratio of ~0.8.

The substrate temperatures reported in Table 3 and shown in the chart in Fig. 2 are estimated from previous calibrations done by melting different metal strips (Al, Ag, Cu, Au) on the substrate heated with the CO_2 laser, as described in [20], and should not be taken as definitive: there is likely an error of ±50 K at the highest values.

Table 3. Deposition Conditions, FMR Linewidth (ΔH), Composition, XRD and Colour of Samples Y8, Y11-Y18[a]

SAMPLE	Estimated substrate temperature [K]	ΔH [mT]	Y at. %	Fe at. %	Y/Fe	YIG peaks in XRD pattern	Sample colour
Y18	300	-	16.0	20.0	0.8	NO	Black
Y17	650	-	17.0	21.5	0.79	NO	Black
Y16	850	-	16.5	22.0	0.75	NO	Dark red
Y15	1000	13.02	17.0	21.0	0.81	YES	Dark yellow
Y14	1150	9.05	17.0	21.0	0.81	YES	Yellow
Y8	1300	4.21	16.5	21.0	0.79	YES	Yellow
Y11	1450	2.91	16.5	21.0	0.79	YES	Yellow
Y12	1600	2.55	17.5	20.5	0.85	YES	Yellow
Y13	1750	3.43	17.0	21.0	0.81	YES	Yellow

[a]The best sample in terms of FMR is highlighted in grey.

XRD analysis showed the presence of diffraction peaks due to the YIG phase only in the samples deposited at a substrate temperature $T \geq 1000$ K, meaning that samples Y16-18, deposited at $T \leq 850$ K, are amorphous, as expected from literature [14,21], and thus do not feature any FMR. Indicators of crystal and magnetic quality of μm-thick YIG films are also their colour, as shown in Table 3, and their optical transmission: YIG films deposited at $T \geq$

#185247 - $15.00 USD Received 12 Feb 2013; revised 14 Mar 2013; accepted 17 Mar 2013; published 16 Apr 2013

1150 K have a light yellow tint and high optical transmission in the visible and near infra-red (NIR), with an absorption edge typically between 450 nm and 550 nm (see Fig. 3); samples deposited at $T \leq 1000$ K have a darker colour, going from dark yellow though red to black as substrate temperature drops, and lower optical transmission with red-shifted absorption edge.

Table 3 and Fig. 2 show a clear correlation between FMR linewidth and substrate temperature, whereas there is no evident correlation between Y concentration and FMR. Figure 2 shows the trend of the FMR linewidth with substrate temperature: once the substrate temperature is high enough to ensure crystallization ($T \approx 1000$ K), FMR is observed for YIG films and the linewidth decreases with increasing temperature until the minimum value (2.55 mT – sample Y12) is reached at $T \approx 1600$ K. This trend also supports our theory, according to which TEC-mismatch plays a role in the relief of strain induced by lattice-mismatch and in the improvement of magnetic properties: in fact, the cooling-down from high substrate temperatures will accommodate the lattice-mismatch-induced stress more easily than the cooling-down from low substrate temperatures.

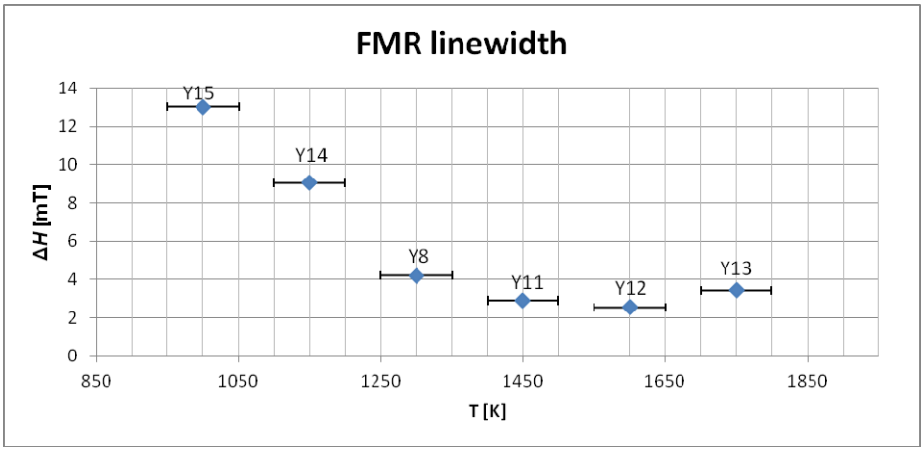

Fig. 2. Variation of FMR linewidth (ΔH) with substrate temperature. ±50 K error bars are shown.

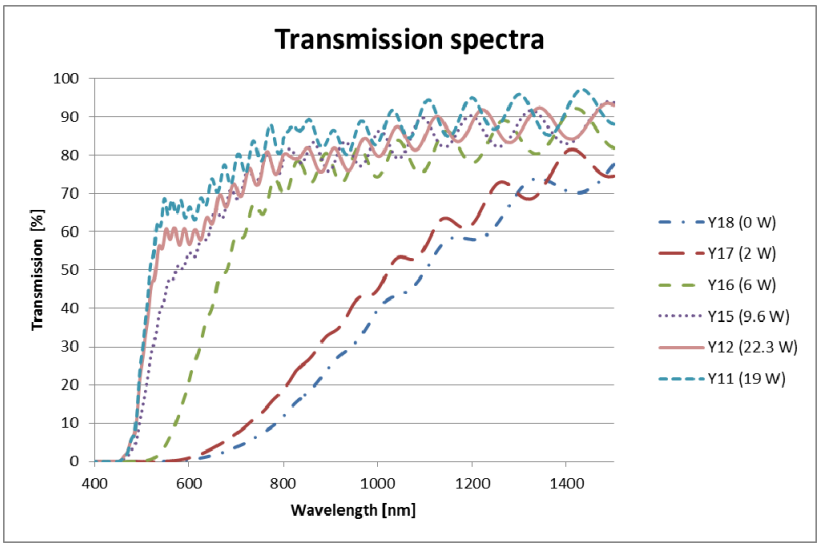

Fig. 3. Transmission spectra of representative samples Y11 and Y15-Y18 Samples Y8, Y13 and Y14 are omitted for clarity, as they lie between those of Y11 and Y15 – Ripples are etalon fringes [22].

#185247 - $15.00 USD Received 12 Feb 2013; revised 14 Mar 2013; accepted 17 Mar 2013; published 16 Apr 2013

3.3 Optimization of oxygen pressure

Samples Y19-Y21 were deposited at the optimum substrate temperature (*T* ≈1600 K) found from the characterization of samples Y11-18 and at different values of oxygen pressure. Table 4 summarizes the results in terms of FMR linewidth, thickness and composition.

Table 4. FMR Linewidth (Δ*H*), Thickness (*t*) and Composition of Samples Y19-Y23[a]

SAMPLE	P_{O2} [Pa]	Δ*H* [mT]	*t* [μm]	Y at. %	Fe at. %	Y/Fe
Y20	1	1.75	2.4	17.0	21.0	0.78
Y19	3.3	2.75	2.5	16.5	21.0	0.79
Y21	6	2.97	1.8	17.0	21.0	0.78

[a]The best sample is highlighted in grey.

According to XRD analysis, all films are crystalline with the same (100) orientation as the YAG (100) substrates. No significant change can be noticed in terms of stoichiometry, when changing the oxygen pressure in the range between 1 and 6 Pa. The best result in terms of FMR linewidth was achieved at P_{O2} ≈1 Pa: Δ*H* = 1.75 mT.

We carried out a few deposition trials at oxygen pressures below 1 Pa, but the broadening of the plume causes a decrease in deposition rate, window coating and consequent decrease in excimer laser fluence and CO_2 laser power, making the study of material properties with changing parameters difficult: variation of crystallinity and magnetic properties cannot be related to just one growth condition and may be due to different factors, such as lower gas pressure, decreasing laser fluence and substrate temperature during the deposition.

Figure 4 shows the XRD pattern of our best sample, Y20: the peaks from the YIG film and the YAG substrate are close to the positions reported in the database [23,24], but suffer instrumental error, which was compensated by shifting the YAG peaks to the database value and then moving the YIG peaks by the same amount, as shown in Table 5: the corrected YAG peak positions are defined as the database positions: $2\theta_{c,YAG\ (x00)} = 2\theta_{d,YAG\ (x00)}$, whereas the measured YIG peak positions are corrected as follows: $2\theta_{c,YIG\ (x00)} = 2\theta_{m,YIG\ (x00)} + (2\theta_{c,YAG\ (x00)} - 2\theta_{m,YAG\ (x00)})$.

Table 5. Database, Measured and Corrected XRD Peak Positions for Y20

XRD peak	Database position $2\theta_d$ [deg]	Measured position $2\theta_m$ [deg]	Corrected position $2\theta_c$ [deg]
YAG (400)	29.8	29.77	29.8
YIG (400)	28.9	28.75	28.78
YAG (800)	61.9	61.78	61.9
YIG (800)	59.9	59.47	59.59

#185247 - $15.00 USD Received 12 Feb 2013; revised 14 Mar 2013; accepted 17 Mar 2013; published 16 Apr 2013

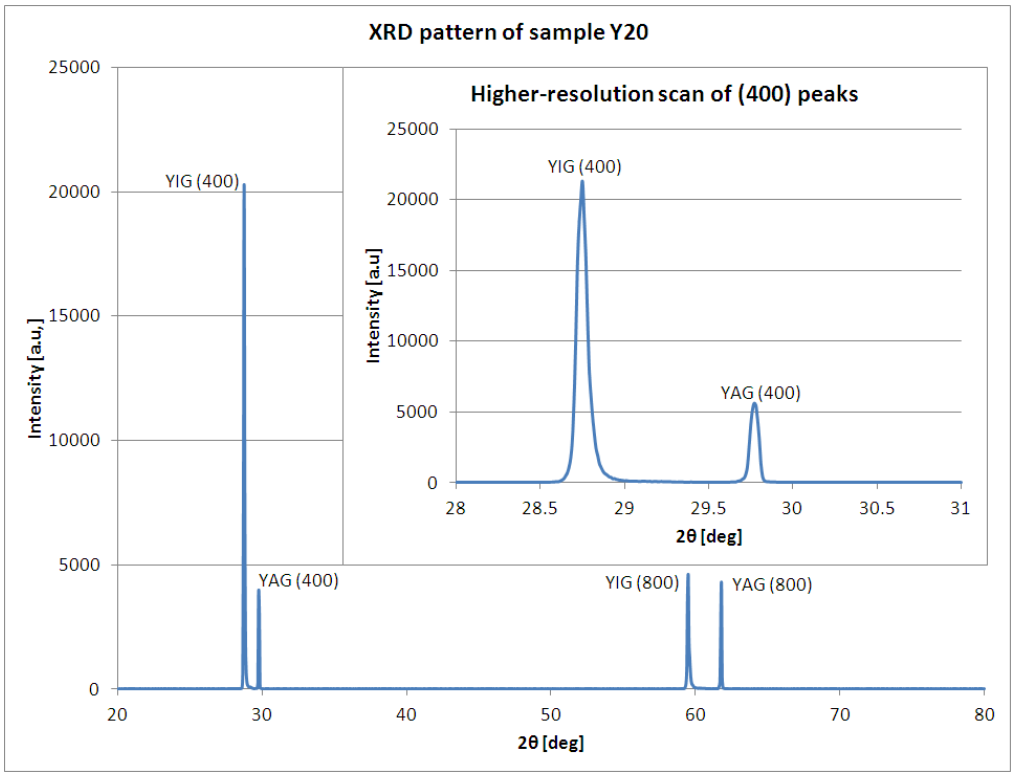

Fig. 4. XRD pattern of Y20. The inset shows a higher resolution scan of (400) peaks.

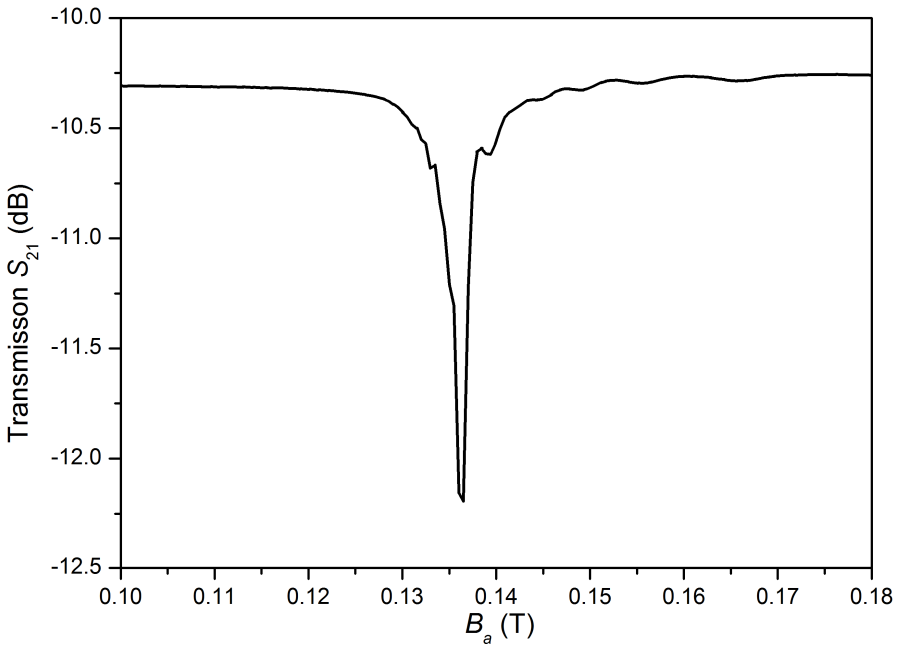

Fig. 5. FMR absorption plot of Y20 at f = 6 GHz.

#185247 - $15.00 USD Received 12 Feb 2013; revised 14 Mar 2013; accepted 17 Mar 2013; published 16 Apr 2013

Figure 5 shows the FMR absorption plot of the best sample, Y20, i.e. the variation of the scattering S-parameter (S_{21}), which is the transmission of microwaves across the sample, as a function of the intensity of the applied magnetic field (B_a). The graph presents a number of satellites to the main FMR resonance peak: these occur at applied fields both greater and less than the main FMR peak and are due to the orientation of the RF excitation field relative to the DC applied field, causing magneto-static modes to be setup [25,26].

4. Conclusion

We have reported the growth of high-quality μm-thick YIG films on YAG substrates by PLD: the films are epitaxial, with the same orientation of the substrate. Compared to YIG films deposited on GGG under the same conditions, YIG/YAG samples feature a narrower FMR linewidth, which suggests that lattice mismatch has a positive effect on the magnetic properties of the YIG films; the mechanism by which the lattice-mismatch causes better magnetic properties has been explained through strain-relief by misfit dislocation and by TEC-mismatch. Substrate temperature and oxygen pressure were optimized at the following values: $T \approx 1600$ K and $P_{O2} \approx 1$ Pa respectively, which allowed us to reach a value of FMR linewidth as low as $\Delta H = 1.75$ mT at $f = 6$ GHz. New multi-PLD experiments are currently in progress to further tune composition and magnetic response of the films by simultaneous ablation of Fe_2O_3 and YIG targets.

Acknowledgments

The research was funded by the Engineering and Physical Sciences Research Council (EPSRC). Grants: EP/F019300/1, EP/G060363/1.

The authors would like to thank Dr. Kate Sloyan in the PLD research group of the Optoelectronics Research Centre of the University of Southampton for discussion and help with PLD, Dr. Mark E. Light in the University of Southampton School of Chemistry for his help with XRD analysis.